Ultrazvočna razpršilna piroliza materialov, na primeru TiO$_2$ nanodelcev

Ultrasonic Spray Pyrolysis Processing of Materials, on the example of TiO$_2$ nanoparticles

Rebeka Rudolf[1, 2], Žiga Jelen[1], Srečko Stopić[3] in Peter Majerič[1,2]

1 University of Maribor, Faculty of Mechanical Engineering, Slovenia

2 Zlatarna Celje d.o.o.

3 RWTH Aachen, IME Institute, Germany

E-Mails: rebeka.rudolf@um.si; z.jelen@um.si; sstopic@ime-aachen.de; peter.majeric@um.si

* Avtor za korespondenco: Rebeka Rudolf, rebeka.rudolf@um.si

Abstract: This article presents new technological advances, trends and the latest scientific results of the bottom-up nanotechnology method called Ultrasonic Spray Pyrolysis (USP) in comparison with other similar processes. USP can produce micro and even nanoparticles from aerosol, which is generated with the use of ultrasound from a chosen solution. Review will show some latest key findings in the field of USP, with the focus of getting a new improved solution, not only in Nanotechnology, but also in a wide range of materials` synthesis, including Micro- and Metastable or Multicomponent forms to increase their transition for special application in different engineering areas in the future. The paper concludes with a presentation of the USP synthesis of TiO2 nanoparticles and their characterization.

Key words: Ultrasonic Spray Pyrolysis; Nanotechnology; TiO2 nanoparticles.

Povzetek: V članku so predstavljeni novi tehnološki pristopi, trendi in najnovejši znanstveni rezultati nanotehnoloških metod od spodaj navzgor, s fokusom na t.i. imenovani ultrazvočni razpršilni pirolizi (USP), v primerjavi z drugimi sorodnimi postopki. USP lahko proizvede mikro in celo nanodelce iz aerosola, ki se tvori z uporabo ultrazvoka iz izbrane raztopine v generatorju. V prispevku bo prikazano stanje in nekatere najnovejše ključne ugotovitve na področju USP, s poudarkom na novih izboljšanih rešitvah, ne samo v nanotehnologiji, temveč tudi v širokem spektru sinteze materialov, vključno z mikro- in metastabilnimi ali večkomponentnimi oblikami za izboljšanje njihovega prenosa specialne uporabe za različna inženirska področja v prihodnosti. Članek zaključujemo s prikazom USP sinteze TiO2 nanodelcev in njihovo karakterizacijo.

Ključne besede: ultrazvočna razpršilna piroliza; nanotehnologija; TiO2 nanodelci.

1. Introduction

Nanotechnology is a branch of science and engineering focused on materials with at least one dimension below 100 nm. Nanomaterials in different form such as: nanoparticles, nanotubes, nanopyramids, etc. have different properties compared to materials with macro dimensions. Their altered physical and chemical properties come from a large surface-to-volume ratio and a high surface activity. Because of this, they are useful in various fields (electronics, chemistry, biotechnology, medicine, cosmetics) [1]. Different production methods for nanoparticles are known, they are divided into bottom-up and top-down approaches. Bottom-up examples include sol-gel, chemical vapour deposition, flame spray synthesis, various pyrolysis and atomic or molecular condensation [2–5]. Top-down methods include laser ablation, nanolithography and high-energy milling [6, 7]. Currently, these methods are suitable for production of small quantities of nanoparticles with major variations in shapes and sizes of the nanoparticles from production of different batches. A bottom-up method, called Ultrasonic Spray Pyrolysis – USP has good potential for removing these technological issues, for a more controlled nanoparticle synthesis [4, 8]. Pyrolysis in general, is a process of chemical decomposition of various compounds at elevated temperatures. With the USP method, we additionally introduce ultrasound for dispersing a precursor solution with our desired material into droplets. These droplets are then exposed to high temperature below 1100°C, such that the material inside the droplet is chemically decomposed via pyrolysis and nanoparticles of pure elements are obtained. The advantage of the USP method is the simplicity of setting up individual process segments and changing their configuration, continuous nanoparticle synthesis and the possibility of synthesizing pure nanoparticles from various materials. The disadvantage is a low efficiency of the method when using an un-optimized USP device used for laboratory purposes (currently around 10%), due to losses of the dissolved material on the construction elements of the USP device.

2. Ultrasonic Spray Pyrolysis

The main elements of the conventional USP device are the ultrasonic generator or nebuliser, the reactor furnace, and a system for nanoparticle collection and cooling (Figure 1). Ultrasonic nebulisers are the most efficient amongst other types of nebulisers, such as pneumatic and electrostatic, while also being affordable and having a low droplet velocity. As such, they are used commonly in spray pyrolysis processes. The sizes of the synthesised nanoparticles depend on the ultrasound frequency [9-11], which determines the sizes of the aerosol droplets, and the concentration of the dissolved salts in the precursor solution droplets. Due to vibrations of the ultrasound below the solution surface, the kinetic energy of the solution molecules increases rapidly. This causes small droplets

to overcome the surface tension and break away from it. This effect, known as nebulisation, produces micron sized aerosol droplets, which act as individual chemical reactors when subjected to thermal treatment [12-13]. Droplets in a size distribution from 1 to 15 micrometres are created with a high-frequency ultrasound (0,5-3 MHz) [14].
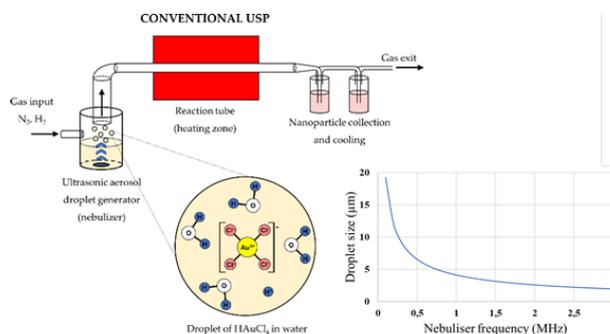
Figure 1. Aerosol droplet formation from starting solution with ultrasound, example of gold chloride precursor for gold nanoparticles synthesis (Assumption: the ion states inside the aerosol droplets are the same as in the starting solution, adapted from [15-16]

The generated droplets of the precursor solution are transported into the furnace with a carrier gas, where the synthesis stages of evaporation and droplet shrinkage, thermal decomposition and densification take place. Depending on the precursor salt composition and chemistry, a reaction gas may be included with the carrier gas to promote the formation of pure metal or metal oxide nanoparticles. The process forms solid, non-porous nanoparticles with different amounts of aggregation, depending on the process parameters used (reaction temperature, residence time, etc.). One classification for nanoparticle synthesis processes is based on the physical state from which the nanoparticles are formed: From the gas, liquid or solid state. Depending on the type of precursor and material synthesised, USP can be categorised in all three states, as nanoparticles can be formed from the gas or the liquid/solid state. Depending on the physical state from which nanoparticles are formed with USP, there are two well-known main conversion routes described in literature [9, 17-18]: the Droplet-To-Particle (DTP) and Gas-To-Particle (GTP) conversion mechanisms. These formation mechanisms can both occur during synthesis with USP, and are determined by the various USP parameters – aerosol droplet size, gas flow, reaction temperatures, precursor solution salt and solvent volatility (ease of vaporisation), etc.

3. Particle formation with USP

3.1. Droplet-To-Particle conversion mechanism in USP

The liquid-to-solid and solid-to-solid conversion processes with USP can be described with the DTP mechanism. This mechanism, in general, consists of the for-

mation of droplets, transportation of these droplets into a heating zone, evaporation of the solvent and thermal conversion of the solute into the final nanoparticles. As the droplet with dissolved material is being evaporated it shrinks, and, simultaneously, increases the mass fraction of the solute inside the droplet. The solute can begin to precipitate before uniform saturation is reached across the droplet because the solute diffusion is slower than the evaporation of the solvent. As the solid material is being precipitated on the droplet surface due to supersaturation, the liquid can become trapped in the centre. It then begins to evaporate through the newly formed surface crust (Figure 2). This slows down the evaporation rate.
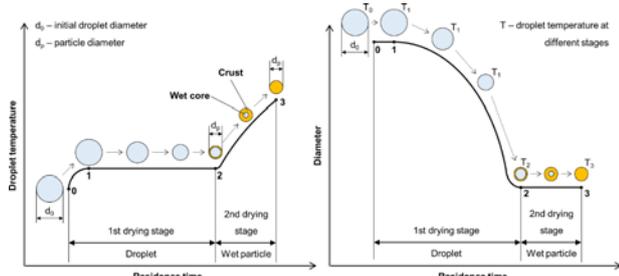
Figure 2. Evaporation of aerosol droplet and drying of the precipitated solute, adapted from [19]

Solute precipitation in droplets has not been described by any theory in a quantitative manner. For a given solute, the supersaturation required for precipitation must be measured [9, 20], and is a function of the exact composition of the solution (impurities act as precipitation sites). Because the rate of nucleation determines particle morphology, the evaporation determines particle morphology (evaporation depends on several factors, such as surrounding vapour pressure and temperature). Intraparticle reactions, such as thermal decomposition, also occur in the aerosol before and after solvent evaporation, and can influence particle morphology (Figure 3). These were studied with thermogravimetric analysis, differential thermal analysis and differential scanning calorimetry [9]. The precursor characteristics determine whether hollow or porous particles are formed. Whether a precursor melts or not before reacting has a very distinct difference on the final nanoparticle morphology. The volume frac-

tion of the solute also influences the formation of porous or hollow particles, as does a high reduction of volume because of reactions.
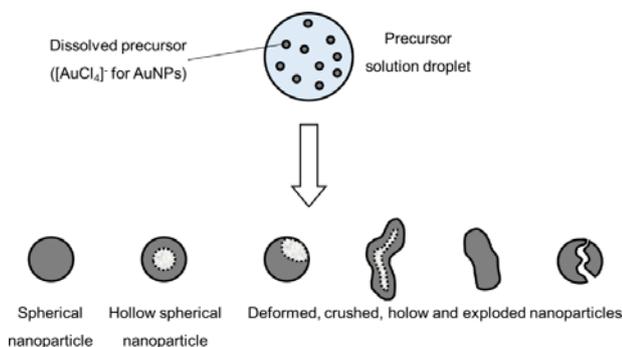
3.2. Gas-To-Particle conversion mechanism in USP

The GTP formation mechanism generally follows the supersaturation of a gaseous species of the desired material, which causes nucleation and new particle formation. The particles can be created by chemical reactions of gaseous precursors, or by physical processes, such as cooling of a hot vapour. The average particle diameter, total particle concentration, size distribution and particle morphology evolve along the aerosol reactor in two different modes. One mode is nucleation-condensation, where a monomer (molecule or atom) is formed by a chemical reaction or a decrease in temperature, until nucleation occurs. The saturation ratio increases, and growth of the monomer proceeds by condensation of the monomer onto the particles. When no collisions occur, they can remain nearly spherical through the aerosol reactor path. Surface reaction on the particles may also occur, promoting growth. Another mode is nucleation-coagulation, where particles are formed and their high concentration allows collisions and coalescence of particles, resulting in growth of the particles. Both modes can be found in laboratory processes, while nucleation-condensation is usually not found in industrial systems.

In the nucleation-condensation mode, the morphology of the particles depends on collisions and coalescence. Particles coalesce by sintering after collisions in order to become spherical. The ratio of rates of collisions and coalescence (αc [9, 22-23]) determines the morphology. In collision-limited growth ($\alpha c = \infty$), the sintering rate is rapid relative to collisions, allowing for the formation of spherical particles between collisions. In sintering-limited growth ($\alpha c = 0$) the particles exist as aggregates. Intermediate conditions ($\alpha c \approx 1$) are in existence in real situations, where the particle morphology is a function of parameters that control the sintering rate – temperature and material properties. The primary particle size is also a function of these parameters (Figure 4).

Figure 3. Types of nanoparticles that can be synthesised from an aerosol droplet, depending on the parameter conditions, adapted from [21]
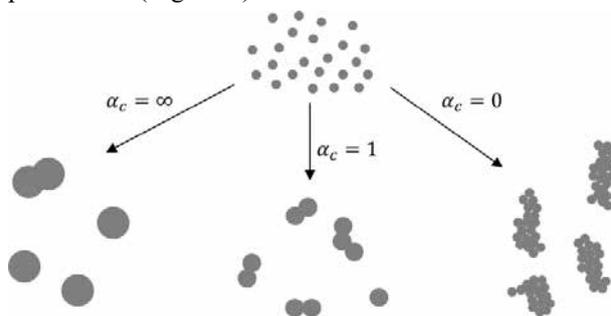
Figure 4. The ratios of collisions and coalescence with the GTP mechanism and the resulting nanoparticle morphologies, adapted from [9, 22-23]

When the aerosol droplet evaporates within the GTP mechanism, the solute is vapourised along with the solvent, resulting in the presence of the solute vapours and their partial vapour pressure. When saturation of vapours is reached, nucleation occurs, and growth of particles proceeds as described previously.

4. Synthesis of TiO$_2$ nanoparticles

In this part some results of the characteristic USP syntheses for TiO$_2$ nanoparticles are presented. The goal of this experimental matrix was to find the influence of the process parameters on the particle size distribution and their morphology. The conducted experiments are presented in Table 1 and 2. The experiments presented in Table 1 are done under a constant temperature profile where the influence of concentration and flow rate were studied. The experiments presented in Table 2 were done with a constant concentration of the precursor solution, where the temperature profile and flow rate were changed and in that way we studied their influence on the nanoparticle characteristics. Lab-scale USP equipment, located in IME Aachen, with R. B. I. GAPUSOL 9001 ultrasonic generator (f= 2,5 MHz) with one transducer was used for the experiments in this research. The TiO$_2$ nanoparticles collection in the conducted experiments was done in the liquid (ethanol) in collecting bottles.

Table 1: Experimental conditions of TiO$_2$ synthesis in USP equipment, with C$_{16}$H$_{16}$O$_4$Ti as a precursor and for the temperature profile 300-800-300°C on the USP equipment

No.	Conc. [mol/l]	Flow N$_2$ [l/min]
T1v	0,025	4
T2v	0,025	5
T3v	0,025	7
T4v	0,0125	4
T5v	0,0185	4
T6v	0,0185	5
T7v	0,0185	7

Table 2: Experimental conditions for synthesis of the TiO$_2$ in the USP equipment from C$_{16}$H$_{16}$O$_4$Ti as the precursor with the concentration 0.0185 [mol/l]

No.	Temp. profile [°C]	Flow N$_2$ [l/min]
T8v	800-800-300	4
T9v	800-800-300	7
T10v	800-800-300	10
T11v	300-800-300	4
T12v	300-800-300	7
T13v	300-800-300	10

*T stands for TiO$_2$, 1-13 is the number of the experiment, v stands for one step USP equipment

Characterization of TiO$_2$ nanoparticles

The TiO$_2$ nanoparticles obtained in the experiments T1$_v$ to T13$_v$ were analysed with the Scanning electron microscopy (SEM) method in order to determine particle morphology and the size distribution. From the presented results (SEM micrographs) it is easy to see that, in most of the experiments, we obtained ideally spherical nanoparticles with smooth surface. In some of the trials, like T8$_v$ to T10$_v$ and T13$_v$ particles with defected structure can also be noticed next to the spherical particles. A close-up is also presented of particles with irregular shape. In the experimental serial T1$_v$-T13$_v$ more process parameters were varied: Concentration, flow rate and temperature profile (see Table 1 and Table 2). Next to the SEM micrographs are presented also the particle size distribution histograms with cumulative distribution.
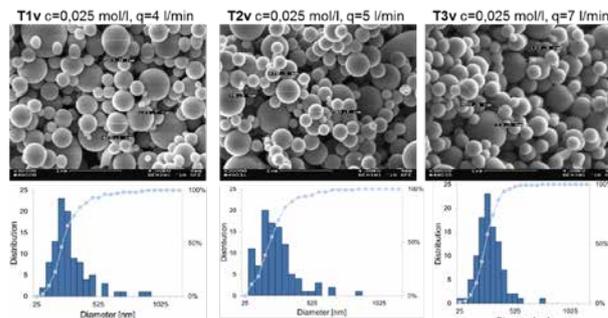
Figure 5: SEM micrographs of TiO$_2$ nanoparticles obtained on the USP equipment at 300°C-800°C-300°C temperature and various carrier gas flow rates with corresponding particle size distributions (experiments T1$_v$ to T3$_v$)

In Figure 5 are presented the SEM micrographs for experiments T1$_v$-T3$_v$ in which the influence of flow rate (and residence time) on the nanoparticle morphology and the size distribution was examined. In the conducted experiments the flow rate showed no significant influence on the TiO$_2$ nanoparticle morphology, since almost all nanoparticles had ideally spherical form. On the other hand, a small influence can be observed on the particle size distribution: the smaller percent of big particles occurs at the higher flow rate. This effect is very small, and it can be considered as a tendency. In all three experiments (T1$_v$-T3$_v$) 50% of the nanoparticles are below 250 nm. For the experiment T1$_v$, 90% of the nanoparticles are below 525 nm, for T2$_v$, 90% are below 500 nm and for T3$_v$, 90% are below 425 nm.
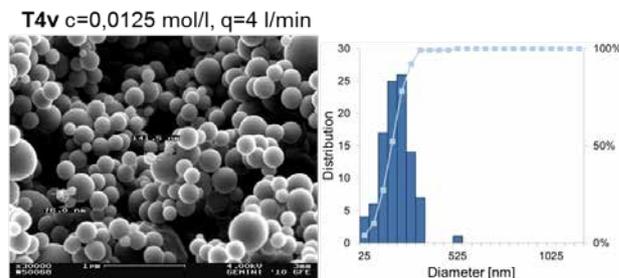
Figure 6: SEM micrographs of TiO$_2$ nanoparticles obtained in experiment T4$_v$ with corresponding particle size distribution

The result of experiment T4$_v$ is presented in Figure 6. The precursor solution concentration used in this experiment gave good results (50% of nanoparticles smaller than 225 nm and 90% smaller than 325 nm), but efficiency and productivity at low concentration was very low. For this reason, no further experiments were done with this concentration. The results presented in Figure 7 are the results of experiments T5$_v$-T7$_v$, which were done under the same process parameters as the experiments T1$_v$-T3$_v$ but with a lower concentration of the precursor solution.

From the results presented in Figure 7, the same tendency can be observed of the influence of the flow rate: No influence on the particle morphology and minimal influence on the particle size distribution. The obtained nanoparticles, as expected due to the lower concentra-
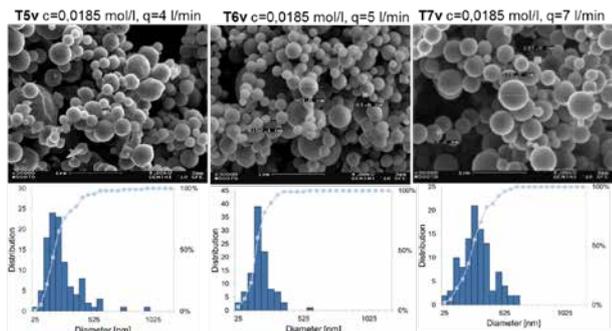
Figure 7: SEM micrographs of TiO$_2$ nanoparticles obtained on the USP equipment at 300°C-800°C-300°C temperatures and various carrier gas flow rate with corresponding particle size distributions (experiments T5$_v$ to T7$_v$)

tion of the precursor solution, are smaller than the ones obtained in the experiments T1$_v$-T3$_v$. It is important to notice that this difference is minimal in the area of nanoparticles smaller than 300 nm (T5v: 50% smaller than 225 nm, T6$_v$: 50% smaller than 220 nm and T7$_v$: 50% smaller than 275 nm). The difference is more obvious in the area of D>500 nm, which means that there are less of the bigger nanoparticles (T5v: 90% smaller than 425 nm, T6v: 90% smaller than 375 nm and T7$_v$: 90% smaller than 450 nm). In the experiments T6$_v$ and T7$_v$, all nanoparticles are below 600 nm. Here is also determined the positive influence of the increased carrier gas flow rate on the nanoparticle size distribution.

The results of characterization for the experiments T8$_v$-T13$_v$ are presented in Figure 8 and Figure 9. Next to the SEM micrographs of obtained nanoparticles are also presented the close-ups of the characteristic structures and the morphological irregularities.
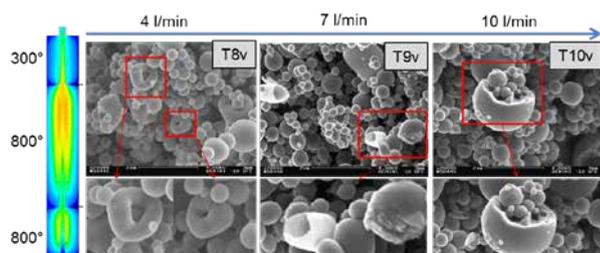
Figure 8: SEM micrographs of TiO$_2$ nanoparticles obtained in the experiments T8$_v$, T9$_v$ and T10$_v$, at a constant precursor solution concentration, 800°C-800°C-300°C temperature and various N2 flow rates, with a close-up of the typical defects (below each SEM micrograph)

Based on the SEM micrographs presented in Figure 8 it is possible to determine that, in all conducted experiments, there was the formation of the various defected nanoparticle morphologies. The reason for this must be the high temperature in the first heating zone (800°C). It is assumed that, in this area, the first two steps of the nanoparticles` formation take place: Evaporation and precipitation. The high temperature in this area obviously has an unwanted effect on the kinetics of the mass and the heat transfers occurring in those formation steps, which is resulting in the various defects in the nanoparticle morphology.
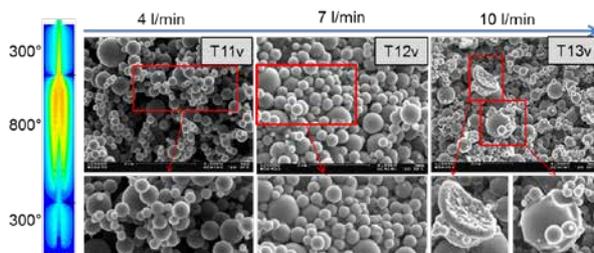
Figure 9: SEM micrographs of the TiO$_2$ nanoparticles obtained in the experiments T11$_v$, T12$_v$ and T13$_v$, at a constant precursor solution concentration), 300°C-800°C-300°C temperature and various N2 flow rates, with the close-up of the typical particle shape and typical defects (below each SEM micrograph)

In the row of the experiments T11$_v$-T12$_v$ the influence was examined of the flow rate and the lower temperature in the first heating zone (300°C) on the nanoparticle formation and the final nanoparticle morphology. The SEM micrographs of the obtained nanoparticles are presented in Figure 9. From the presented micrographs it is possible to see, that the lower temperature in the first heating zone and moderate carrier gas flow rate have a positive influence on the formation of ideally spherical nanoparticles, as shown in the experiments T11$_v$ and T12$_v$. The SEM micrographs of the nanoparticles obtained in the experiment T13v show that, even at the lower temperature in the first heating zone, the high carrier gas flow rate can lead to the formation of the defected nanoparticle morphology.

By comparing the results presented in Figure 8 and Figure 9, especially the one from the experiment T8v with the one from T11$_v$, and T9$_v$ with the one from T12$_v$, it is clear to see that the temperature profile plays
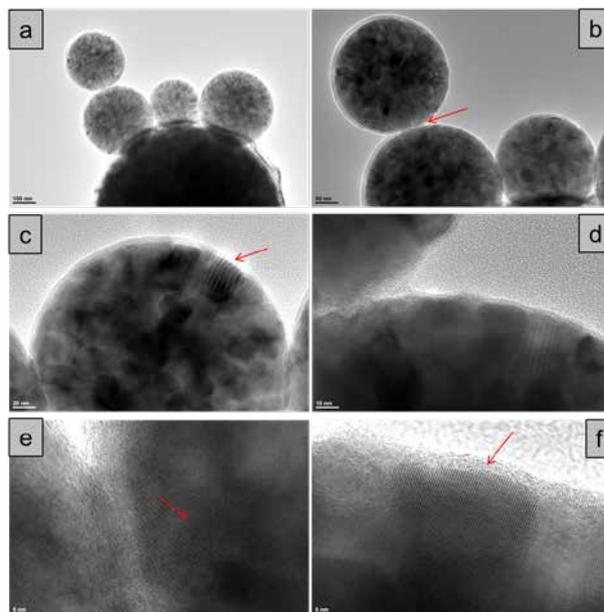
Figure 10: TEM analysis of the TiO$_2$ nanoparticles obtained in the experiment T12$_v$, a- spherical nanoparticles, b- detail showing that the individual nanoparticles are building the soft agglomerates, c- and d- polycrystalline structure of individual nanoparticles with the visible primary nanoparticles and some examples of the defects in the primary nanoparticle structure (twins), e- the structure of the primary nanoparticles, f- clearly apparent nanocrystallite of approximately 10-15 nm size

a more important role in the particle formation and the morphology than the carrier gas alone. The first heating phase, as assumed already, has the deciding influence on it. A detailed discussion about those results will be presented in the model proposal and the model validation part.

The nanoparticles obtained in the experiment T12$_v$ were analysed additionally by Transmission Electron Microscopy (TEM), the results of TEM analysis are presented in Figure 10 where the particle morphology and substructure of the primary nanoparticles can be better observed.

From Figure 10 it is easy to see that the individual secondary nanoparticles have the size 200-600 nm. They are building soft agglomerates that can be separated easily by mechanical dispersion. The secondary nanoparticles are built up from the primary particles that have irregular shape, are mono-crystalline and have a size in the range 5-20 nm. In the presented results (c-f) it is possible to see the primary particles, grain boundaries, structural defects (twins) and crystal structure. On the presented results it is possible to see the presence of a Moire frame (fringe) which indicates that the structure of the synthesized nanoparticles is not fully furnished and contains a high concentration of defects. Further information, which can be collected from the obtained results, is that it came to more or less uniform precipitation during the process of synthesis of those nanoparticles (in the presented experiment), since there is no visible concentration gradient from the centre of the particle to its surface. This can be concluded at least for the four fully visible nanoparticles, whereas the biggest nanoparticle is not fully visible and this conclusion can't be transferred to it directly.

5. Discussion

The SEM and TEM micrographs of the obtained TiO$_2$ nanoparticles show that most of the nanoparticles (90%) are in the size range from 50 nm up to 500 nm, whereas a small percentage (less than 10%) is in the sub-micrometre to micrometre size range. In addition, the results have showed that over 90 % of the TiO$_2$ nanoparticles have spherical form and a dense structure, whereas less than 10% had shown defects in the structure and a hollow morphology. In order to explain these differences in the particles` morphology and relatively bright size range (also in the case of the same experiment), it was necessary to determine which droplets come due to the surface precipitation and which to the volume precipitation in the evaporation/precipitation step. The nanoparticles bigger than 500 nm have showed that for an explanation of their formation, especially in the evaporation/precipitation step, the classical model has to be upgraded. This new analysis of the DTP transformation route, with the

accent on the evaporation/precipitation step, is going to be conducted by the investigation of the temperature gradient inside the droplet and the Biot number (Bi number) [24], which is a dimensionless quantity used in calculating heat transfer. It is explained that when $0,1 < Bi < 40$, the internal and external resistance to heat transfer are almost the same (so that both are important). In the case of the conducted experiments, the droplet and the fluid are both flowing, and for all experiments the calculated value of the Bi number was around 0,275. From this information it is possible to conclude that there does exist the resistance to conductive heat transfer in the droplet in the evaporation/precipitation stage and, as the result of it, the temperature gradient inside the droplet does exist.

Based on the calculated values for the Biot number, in the case for both the applied equipment, and independently of the droplet size in the range 1-15 µm, it can be determined that the temperature gradient exists in all the droplets. The existence of the temperature gradient inside the droplet leads to the formation of a concentration gradient inside of it, since the temperature has direct influence on the kinetic of mass transfer processes inside the droplet (diffusion). On the other hand, this indicates that all the droplets might undergo the surface precipitation process, since one of the conditions for such a precipitation is the concentration gradient. One part of the adaptation of the classical model is that it is assumed that the model must be slightly different in the case of the smaller and bigger droplets, due to the difference in the length of the diffusion way, since it plays one of the main roles in the droplet-to-particle transformation and the final nanoparticle morphology. In the very small droplets (1-3 µm), the temperature gradients are very small and also the concentration gradients, so that in those cases the volume precipitation can take place. In the case of the small droplets (3-8 µm), in the evaporation/precipitation step, the evaporation of the liquid from the droplet surface is a much faster process compared to the diffusion of the solid and liquid inside the droplet. Since the evaporation leads to a fast increase of the precursor concentration on the droplet surface, this is the place where the precipitation starts. With the further solvent evaporation, the precipitation front moves towards the droplet/particle centre. Since the diffusion of solute from the centre of the droplet is not fast enough, not all the solute manages to reach all the way to the surface and, in this way, the precipitation front ends in the centre of the particle. This results in a dense nanoparticle morphology, even though the surface precipitation took place. It is in a way a special case of the surface precipitation. In the case of the bigger droplets (8-15 µm), the evaporation of the droplets also takes place on the droplet surface and the formation of the

concentration gradient follows the same trend as the one for the smaller droplets, but in this case the distance that the precipitation front needs to make from the droplet surface to the centre is much bigger and, for this, much more relevant. In this case, the precipitation also starts on the droplet/particle surface, the precipitation front moves towards the droplet centre, and the diffusion goes from the centre to the surface. Due to the length of the way of the diffusion path and the precipitation moving path, those two lines meet at some distance away from the droplet centre (see Figure 11). The movement of the precipitation front is faster than the diffusion. In this case, the more or less hollow particles will be formed, where the thickness of the wall of the particles depends on the precursor solution physical characteristics and the process parameters. It is expected that, for this droplet size, the precipitation front met the diffusion front at 80% of the full distance from the surface to the centre. For this reason, it is expected that the wall thickness is at least 80% of the particle diameter. For the droplet with the size bigger that 15 μm the same processes take place, but due to the longer distance from the surface to the centre, bigger particles with a thinner wall thickness will be formed (see Figure 11). In the case that the wall is not permeable for the evaporated gas diffusion, it might result in the wall breaking and the formation of so-called exploded particles.
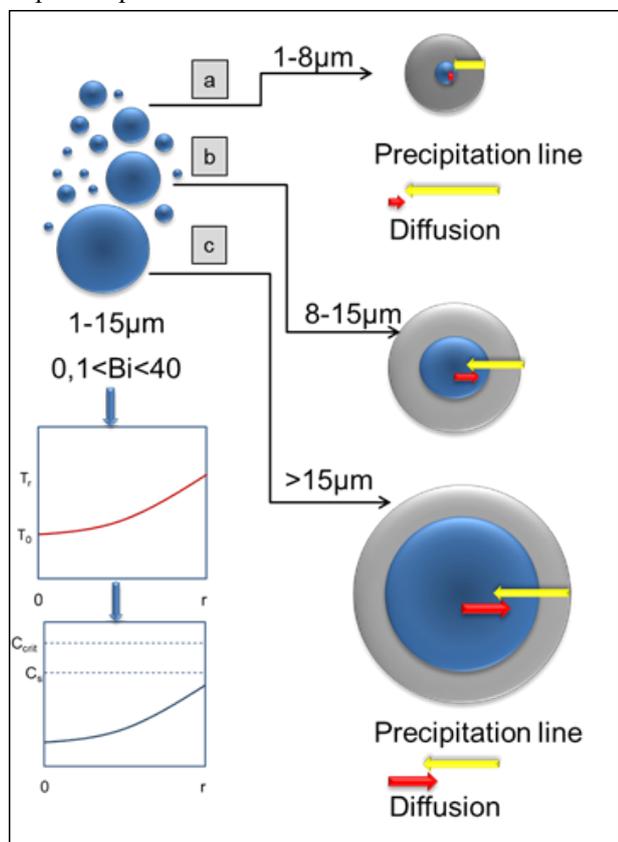
Figure 11: Adapted model for D-T-P transformation pathways for the big and the small droplets

From the presented discussion and model adaptation, it is easy to conclude that it is not possible to avoid the formation of temperature and concentration gradient inside the droplet completely, but it is possible to influence the pathways and kinetic of particle formation (with a droplet size and process parameters like flow rate and temperature) and in this way influence partly the particle morphology.

From the model presented in Figure 11 it is easy to see that, for all droplets, the temperature and concentration gradients are assumed, and that the deciding factor that defines the particle formation and morphology is the droplet size. On the other hand, the other parameters, such as the flow rate and the temperature, also have very important influence on the end particle morphology. This influence can be the best observed from the experimental results obtained in the experiments T8$_v$ to T13$_v$, presented in Figure 12.
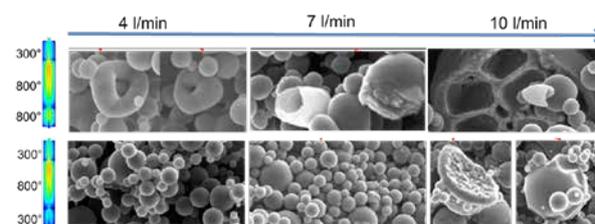
Figure 12: Typical morphology and defects of TiO$_2$ nanoparticles obtained in the experiments T8$_v$ to T13$_v$, showing the influence of the temperature and the flow rate on the nanoparticle morphology

In the example presented in Figure 12 it is easy to see that, if the volume flow and temperature in the zone where the evaporation/precipitation step takes place increase, the evaporation rate on the droplet surface increases and defects like the ones presented in Figure 12 may occur. This kind of behaviour is expected from the very beginning, since it is the behaviour partly predicted with the known D-T-P model. Based on the results of this research, it is concluded that defected particles are formed only in the case of bigger droplets (>8μm), especially for >15μm. This means that the adapted model, presented in Figure 11, is connected also to influences of the extreme flow rate/temperature and must be implemented in it. By overall assessment of the experimentally obtained results, it may be concluded that the theoretical D-T-P model, after the presented adaptation, corresponds to the experimental results. The experimental results gave a deeper understanding of the complex correlation of the process parameters and enabled better control of them.

6. Conclusions

From the presented review the following conclusions can be summarised:

It is important to take into account that the USP is a very fast process where all the described processes

take place in micrometers' volume and in parts of seconds. For these reasons, the deviations of the proposed models are possible, and based on this, synthesised nanoparticles are very often in a metastable state.

TiO$_2$ nanoparticles were synthetized, and all the experimental results have indicated that, for the applied process, the classical D-T-P model does not sufficiently describe the particle formation mechanism. Based on this experience, the adaptation of the known D-T-P model was done.

By the right choice of the mentioned process USP parameters it is possible to produce ideally spherical, polycrystalline and dense nanoparticles.

Acknowledgments

References

1. V. V. Mody, R. Siwale, A. Singh, and H. R. Mody, "Introduction to metallic nanoparticles," *J. Pharm. Bioallied Sci.*, vol. 2, no. 4, pp. 282–289, 2010.

2. Y.-C. Wang and S. Gunasekaran, "Spectroscopic and microscopic investigation of gold nanoparticle nucleation and growth mechanisms using gelatin as a stabilizer," *J. Nanoparticle Res.*, vol. 14, no. 10, pp. 1–11, Sep. 2012.

3. R. G. Palgrave and I. P. Parkin, "Aerosol Assisted Chemical Vapor Deposition of Gold and Nanocomposite Thin Films from Hydrogen Tetrachloroaurate(III)," *Chem. Mater.*, vol. 19, no. 19, pp. 4639–4647, Sep. 2007.

4. T. T. Kodas and M. J. Hampden-Smith, *Aerosol Processing of Materials*, 1 edition. New York: Wiley-VCH, 1998.

5. J. Kimling, M. Maier, B. Okenve, V. Kotaidis, H. Ballot, and A. Plech, "Turkevich Method for Gold Nanoparticle Synthesis Revisited," J. Phys. Chem. B, vol. 110, no. 32, pp. 15700–15707, Aug. 2006.

6. N. G. Bastús, J. Comenge, and V. Puntes, "Kinetically Controlled Seeded Growth Synthesis of Citrate-Stabilized Gold Nanoparticles of up to 200 nm: Size Focusing versus Ostwald Ripening," Langmuir, vol. 27, no. 17, pp. 11098–11105, Sep. 2011.

7. G. Schmid and B. Corain, "Nanoparticulated Gold: Syntheses, Structures, Electronics, and Reactivities," Eur. J. Inorg. Chem., vol. 2003, no. 17, pp. 3081–3098, 2003.

8. G. L. Messing, S.-C. Zhang, and G. V. Jayanthi, "Ceramic Powder Synthesis by Spray Pyrolysis," J. Am. Ceram. Soc., vol. 76, no. 11, pp. 2707–2726, Nov. 1993.

9. Kodas, T.T.; Hampden-Smith, M.J. Aerosol Processing of Materials; 1 edition.; Wiley-VCH: New York, 1998; ISBN 978-0-471-24669-5.

10. Messing, G.L.; Zhang, S.-C.; Jayanthi, G.V. Ceramic Powder Synthesis by Spray Pyrolysis. Journal of the American Ceramic Society 1993, 76, 2707–2726, doi:10.1111/j.1151-2916.1993.tb04007.x.

11. Xiong, Y.; Kodas, T.T. Droplet evaporation and solute precipitation during spray pyrolysis. Journal of Aerosol Science 1993, 24, 893–908, doi:10.1016/0021-8502(93)90069-L.

12. Bang, J.H.; Suslick, K.S. Applications of Ultrasound to the Synthesis of Nanostructured Materials. Adv. Mater. 2010, 22, 1039–1059, doi:10.1002/adma.200904093.

13. S. Suslick, Y.D. Acoustic Cavitation and Its Chemical Consequences. Philosophical Transactions of the Royal Society A: Mathematical, Physical and Engineering Sciences 2000, 357, doi:10.1098/rsta.1999.0330.

14. Bogović, J.; Schwinger, A.; Stopic, S.; Schröder, J.; Gaukel, V.; Schuchmann, H.P.; Friedrich, B. Controlled droplet size distribution in ultrasonic spray pyrolysis. Metall 2011, 65, 455–459.

15. Stopic, S.; Rudolf, R.; Bogovic, J.; Majerič, P.; Čolić, M.; Tomić, S. Synthesis of Au nanoparticles prepared by ultrasonic spray pyrolysis and hydrogen reduction. Materiali in Tehnologije 2013, 47, 577–583.

16. Majerič, P.; Jenko, D.; Budič, B.; Tomić, S.; Čolić, M.; Friedrich, B.; Rudolf, R. Formation of Non-Toxic Au Nanoparticles with Bimodal Size Distribution by a Modular Redesign of Ultrasonic Spray Pyrolysis. Nanoscience and Nanotechnology Letters 2015, 7, 920–929, doi:10.1166/nnl.2015.2046.

17. Eslamian, M.; Ahmed, M.; Ashgriz, N. Modeling of Solution Droplet Evaporation and Particle Evolution in Droplet-to-Particle Spray Methods. Drying Technology 2009, 27, 3–13, doi:10.1080/07373930802565665.

18. Tsai, S.C.; Song, Y.L.; Tsai, C.S.; Yang, C.C.; Chiu, W.Y.; Lin, H.M. Ultrasonic spray pyrolysis for nanoparticles synthesis. Journal of Materials Science 2004, 39, 3647–3657, doi:10.1023/B:JMSC.0000030718.76690.11.

19. Mezhericher, M.; Levy, A.; Borde, I. Heat and mass transfer of single droplet/wet particle drying. Chemical Engineering Science 2008, 63, 12–23, doi:10.1016/j.ces.2007.08.052.

20. Hileman jr., O.E. Precipitation from homogeneous solution applied to the drop technique for the study of nucleation. Talanta 1967, 14, 139–140, doi:10.1016/0039-9140(67)80061-4.

21.   Draper, N.D. Investigation of Surface-Potential Controlled Nucleation Using an Acoustic Levitation Apparatus. Thesis, Science: Department of Chemistry, 2012.

22.   Wu, M.K.; Windeler, R.S.; Steiner, C.K.R.; Börs, T.; Friedlander, S.K. Controlled Synthesis of Nanosized Particles by Aerosol Processes. Aerosol Science and Technology 1993, 19, 527–548, doi:10.1080/02786829308959657.

23.   Kruis, F.E.; Kusters, K.A.; Pratsinis, S.E.; Scarlett, B. A Simple Model for the Evolution of the Characteristics of Aggregate Particles Undergoing Coagulation and Sintering. Aerosol Science and Technology 1993, 19, 514–526, doi:10.1080/02786829308959656.

24.   Bogovic, Jelena. Synthesis of the oxide and metal/oxide nanoparticles by the Ultrasonic Spray Pyrolysis : degree of doctor of engineering. [Aachen: J. Bogovic], 2014.